RSC Advances

PAPER

View Article Online
View Journal | View Issue

Cite this: *RSC Adv.*, 2025, **15**, 27544

Investigating the potent antimicrobial properties of a supramolecular Zn(II)-metallogel formed from an isophthalic acid-based low molecular weight gelator

Subhendu Dhibar,*[a] Sangita Some,[a] Suchetana Pal,[b] Rajlakshmi Laha,[b] Priya Kaith,[c] Aditi Trivedi,[d] Subham Bhattacharjee,[e] Lebea N. Nthunya,[f] Timothy O. Ajiboye,[g] Sumit Kumar Panja,[h] Asit Kumar Das,[i] Ashok Bera,[c] Somasri Dam*[b] and Bidyut Saha*[a]

A zinc(II)-based metallogel was synthesized using isophthalic acid as a gelator in *N*,*N*-dimethylformamide at room temperature. The gel formation was confirmed by FT-IR spectroscopy, revealing coordination interactions responsible for network assembly. Rheological studies demonstrated the mechanical robustness and stability of the Zn(II)-metallogel under various conditions. Field emission scanning electron microscopy (FESEM) and energy-dispersive X-ray (EDX) mapping analyses revealed a well-defined microstructure and uniform elemental distribution, providing insight into its morphology and composition. Antimicrobial evaluations showed notable inhibitory effects against both Gram-positive and Gram-negative bacterial strains, underlining the metallogel's broad-spectrum efficacy. These results indicate that the Zn(II)–isophthalic acid metallogel holds strong promise for applications in antimicrobial materials. Its structural integrity and bioactivity suggest potential utility in biomedical and industrial domains, promoting the development of advanced multifunctional materials.

Received 24th May 2025
Accepted 28th July 2025

DOI: 10.1039/d5ra03663a

rsc.li/rsc-advances

1. Introduction

Gels are fascinating soft materials composed of a three-dimensional network of polymeric or molecular frameworks that trap large quantities of solvent within their structure.[1] This immobilization of solvents is primarily facilitated by gelator molecules that interconnect through various forms of cross-linking, forming a stable matrix.[2] The formation of gels often defies predictability and can occur through serendipitous pathways, making their design and synthesis a subject of ongoing intrigue in materials chemistry.[3] A widely used method to confirm gel formation is the "inversion test," where a sample's ability to retain its shape against gravitational force upon inverting the container is visually assessed.[3]

Gels pervade our daily lives and are integral to numerous products, ranging from personal care items like soaps, shampoos, and cosmetics to biomedical devices such as contact lenses and topical drug formulations. Their diverse applications reflect the importance and adaptability of these soft materials in both industrial and consumer sectors.[4]

Broadly, gels are categorized based on the nature of interactions that establish their network structure. Chemical gels are formed through permanent covalent bonds, imparting high mechanical stability and irreversibility.[5] In contrast, supramolecular gels are formed by reversible, non-covalent interactions among low molecular weight gelators (LMWGs), which generally have molecular weights below 3000.[6,7] These gels assemble *via* a variety of weak forces, such as hydrogen bonding, π···π interactions, van der Waals forces, electrostatic interactions, hydrophobic effects, dipole–dipole interactions, and π-system stacking.[8–13] The reversible and dynamic nature of these forces enables supramolecular gels to exhibit remarkable properties such as self-healing, responsiveness to external stimuli, and sol–gel phase reversibility.

[a]*Colloid Chemistry Laboratory, Department of Chemistry, The University of Burdwan, Golapbag, Burdwan 713104, West Bengal, India. E-mail: sdhibar@scholar.buruniv.ac.in; bsaha@chem.buruniv.ac.in; Tel: +91 7001575909; +91 9476341691*

[b]*Department of Microbiology, The University of Burdwan, Burdwan 713104, West Bengal, India. E-mail: sdam@microbio.buruniv.ac.in*

[c]*Department of Physics, Indian Institute of Technology Jammu, J & K-181221, India*

[d]*National Institute of Science Education and Research (NISER), Bhubaneswar, Odisha 752050, India*

[e]*Department of Chemistry, Kazi Nazrul University, Asansol 713303, West Bengal, India*

[f]*Institute for Nanotechnology and Water Sustainability, University of South Africa, Florida Science Campus, 1709 Roodepoort, South Africa*

[g]*Faculty of Natural and Agricultural Sciences, North-West University, Mmabatho 2735, South Africa*

[h]*Tarsadia Institute of Chemical Science, Uka Tarsadia University, Surat 394350, Gujrat, India*

[i]*Department of Chemistry, Murshidabad University, Berhampore 742101, West Bengal, India*

Numerous small organic molecules have been identified as effective LMWGs, including dicarboxylic acids,[14] urea derivatives,[15] modified amino acids,[16] fatty acids,[5] sorbitol,[17] dendrimers,[17] carbohydrates,[17] and more. The molecular structure and functional groups present in these gelators play a critical role in determining their assembly behavior and gelation efficiency. Moreover, the solvent environment is equally pivotal. Solvent polarity, viscosity, and interaction with gelators significantly influence the morphology and mechanical properties of the resulting gel. A wide variety of solvents, both organic and inorganic, are used to initiate gel formation. Commonly employed solvents include water,[18] alcohols,[19] dimethylformamide (DMF),[20] dimethyl sulfoxide (DMSO),[21] acetonitrile,[22] acetone,[23] are among the most effective solvents for initiating supramolecular gel formation. In some cases, the solvent itself may act as a co-gelator, aiding in the structural assembly through non-covalent interactions.

The reversible transformation between gel and sol states, influenced by variables such as temperature, pH, ionic strength, and mechanical stress, allows these materials to adapt and respond to external cues.[24] This responsiveness has paved the way for a broad spectrum of applications, including but not limited to drug delivery,[25] tissue scaffolding,[26] catalysis,[18a,b] environmental remediation,[27] and soft robotics.[28]

A particularly intriguing subset of supramolecular gels is metallogels, which involve the integration of metal ions or metal complexes into the gel network.[29] These materials are formed through coordination between LMWGs and transition metals, resulting in hybrid structures with enhanced functional properties. Transition metals such as Cu(II),[30] Ni(II),[31] Co(II),[32] Zn(II),[33] Fe(II/III),[34] Cd(II),[35] Hg(II),[35,36] and Mn(II)[29] have been extensively used in metallogel synthesis. The incorporation of metal ions not only strengthens the gel network but also imparts additional functionalities such as redox activity,[37] catalytic behavior,[18] and magnetic responsiveness[38] and nanoparticle templating.[39] Among these, Zn(II)-based metallogels are particularly noteworthy due to their multifunctionality. They have shown promise in various fields including chemical sensing,[40] drug delivery,[41] anticancer therapies,[42] cell imaging,[43] dye adsorption,[44] and materials with self-healing abilities.[45]

Metallogels can inhibit the growth of bacteria through different mechanisms. Metallogels can disrupt the membrane of bacteria, which results in intracellular components leaking out from the cell.[46] Metallogels can produce oxidative stress in bacteria leading to the formation of reactive oxygen species (ROS) that can degrade bacterial DNA, proteins, and lipids.[47] A metal and polyphenol-based gel has shown promise in wound healing applications.[48] The antimicrobial activity of nickel(II) and zinc(II) metallogels offers a potential defense against various bacteria that infect humans.[49] Silver nanoparticle-infused peptide nanofibers show promise as an antimicrobial nanohybrid gel.[47] The incorporation of nickel, zinc, or cadmium ions into suberic acid-based metallogels can prevent bacterial growth.[50] Zinc ions are necessary for cellular processes at minimal concentrations, but at higher levels, they can be detrimental. Concentration dependent hemolytic activity to RBC was observed as an effect of zinc oxide nanoparticles.[51] Zinc ions effectively suppressed the growth of B16, HeLa, and I-221 cell lines.[52] In a significant advancement, Dhibar and colleagues[18,20] reported a straightforward and efficient method for synthesizing metallogels that eliminates the need for harsh reaction conditions while preserving their functional properties. Building upon this approach, we successfully developed a room-temperature-stable metallogel by employing isophthalic acid as the sole low molecular weight gelator (LMWG) and zinc(II) as the transition metal source, using *N*,*N*-dimethylformamide as the solvent. The Zn(II)-metallogel (Zn-IPA) was synthesized under ambient conditions through a simple, ligand-free protocol without the need for any additional supporting agents. Rheological analysis and microstructural characterization were conducted to evaluate the gel's physical properties. Notably, this metallogel exhibited strong antibacterial activity against various pathogenic microorganisms. Zn-IPA was particularly effective against both Gram-positive and Gram-negative bacteria, highlighting its multifunctional potential.

2. Experimental

2.1. Materials

Zinc(II) acetate dihydrate (99.995%), isophthalic acid (99%) and trimethylamine (anhydrous, ≥99%) were purchased from Sigma-Aldrich and utilized as received. Throughout the study dry DMF solvent was utilized. Commercially available DMF (purchased from SRL) was dried by using calcium hydride (~1.5 g/100 ml) for six hours at room temperature. After the drying process the intermediate fraction was collected and kept on activated molecular sieves to preserve the anhydrous condition. We purchased yeast extract powder, tryptone and D-(+)-glucose anhydrous from Himedia. The acetone and ethanol used in our device fabrication were of analytical reagent (AR) grade with a purity of ≥99.5%, procured from Sigma-Aldrich. Distilled water was freshly prepared in our laboratory using a double-distillation apparatus.

2.2. Synthesis of Zn(II)-isophthalic acid based metallogel (Zn-IPA)

A stable white Zn-IPA metallogel was synthesized by quickly mixing 500 μL of zinc acetate (0.219 g, 1 mmol) and 500 μL of isophthalic acid (0.332 g, 2 mmol) in DMF, in the presence of 0.2 ml trimethylamine. The mixture was then subjected to continuous ultrasonication in a water bath for 10 minutes (Fig. 1). This process facilitated the formation of a supramolecular network through non-covalent interactions between Zn^{2+} ions and isophthalic acid within the DMF medium. Ultrasonication enhanced molecular mixing and accelerated the self-assembly of the gel components, leading to the formation of a stable three-dimensional metallogel structure. The resulting Zn-IPA gel exhibited excellent stability and uniformity, making it a suitable candidate for applications requiring robust supramolecular materials (Fig. 1). To assess the minimum critical gelation concentration (MGC) of Zn-IPA, the concentrations of zinc acetate dihydrate [$Zn(CH_3COO)_2 \cdot 2H_2O$] and isophthalic acid were systematically varied within the range of 30–550 mg

ml^{-1}, while maintaining a constant weight ratio of 1 : 2 for Zn(II) salt to isophthalic acid. Gelation was tested in the presence of 0.2 ml trimethylamine base in DMF. A stable, white Zn-IPA metallogel was successfully formed at a concentration of 550 mg ml^{-1}, indicating this as the MGC required to achieve a self-supporting, three-dimensional supramolecular network.

2.3. Apparatus and measurements

2.3.1. Ultra-sonication process. The synthesis of the metallogel was carried out using a Phoenix Digital Ultrasonic Cleaner (Model: PHUC-150).

2.3.2. Rheological analysis. The rheology experiments were performed upon fixing the gap distance between the cone and the plate at 0.5 mm. The gels were scooped on the plate of the rheometer. An oscillatory strain amplitude sweep experiment was performed at a constant oscillation frequency of 1 Hz for the applied strain range 0.001–100% at 25 °C. Oscillatory frequency sweep experiments were performed in the linear viscoelastic region (strain 0.01%) to ensure that calculated parameters correspond to intact network structures.

2.3.3. Field emission scanning electron microscopic (FESEM) study. The metallogel was carefully drop-cast on top of the freshly cleaned glass surface and allowed to air-dry overnight. The samples were then coated with gold vapor and analyzed on a Carl Zeiss SUPRA 55VP instrument operated at 10–15 kV and a ZEISS EVO 18 device was used for energy-dispersive X-ray spectroscopy (EDX) investigation.

2.3.4. FT-IR study. IR spectra in the 4000–500 cm^{-1} range of the samples pelleted in KBr were recorded either on a JASCO FTIR 4700 spectrophotometer.

2.4. Antimicrobial activity of metallogel

The inhibitory effect of metallogel Zn-IPA on various bacterial strains was investigated. A series of different metallogel concentration (20 mg ml^{-1}, 40 mg ml^{-1}, 60 mg ml^{-1}, 80 mg ml^{-1} and 100 mg ml^{-1}) was prepared with deionized water (Merck Millipore, France) to form a suspension. Antibacterial efficacy was assessed against Gram-positive bacteria *Bacillus subtilis* (*B. subtilis*), *Staphylococcus epidermidis* (*S. epidermidis*) and Gram-negative *Escherichia coli* (*E. coli*), *Pseudomonas aeruginosa* (*P. aeruginosa*). A broad-spectrum antibiotic, streptomycin (100 μg ml^{-1}), was used as a positive control. TGE agar was used as the growth medium, which contains 1% tryptone, 1% glucose, and 1% yeast extract, all at a pH of 6.5. Sterile cotton swabs were used to distribute 100 μL of each log-phase bacterial culture evenly across the surface of the agar

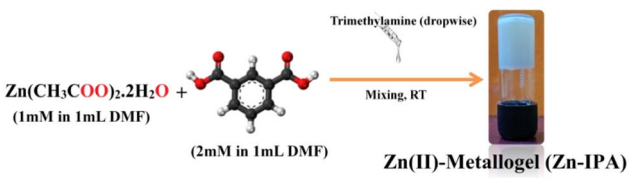

Fig. 1 Synthesis of the Zn-IPA metallogel and visual demonstration of its gelation through the inverted vial test.

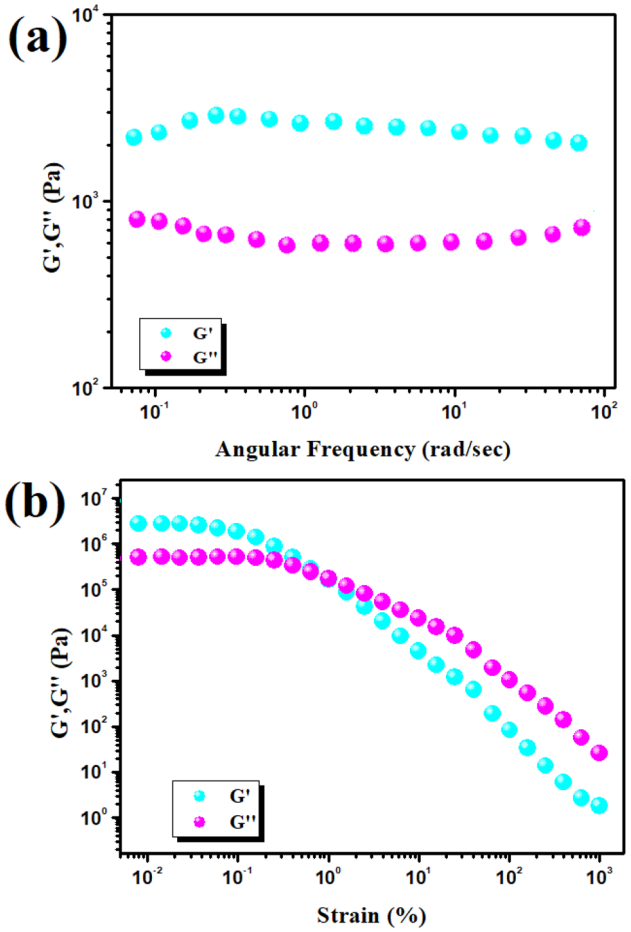

Fig. 2 (a) Variation of storage modulus (G') and loss modulus (G'') of the Zn(II)-metallogel as a function of angular frequency; (b) strain-sweep analysis of the Zn(II)-metallogel performed at a constant angular frequency of 6.283 rad s^{-1}.

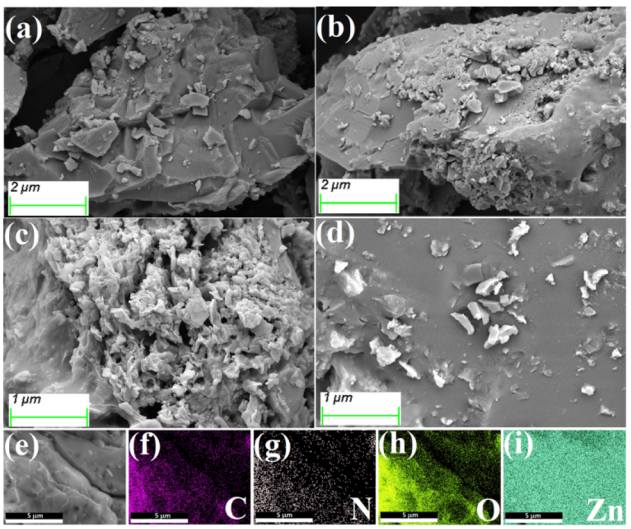

Fig. 3 (a–d) FESEM images showing the microstructural features of the Zn-IPA metallogel; (e–i) Elemental mapping confirms the uniform distribution of C, N, O, and Zn elements within the Zn-IPA metallogel.

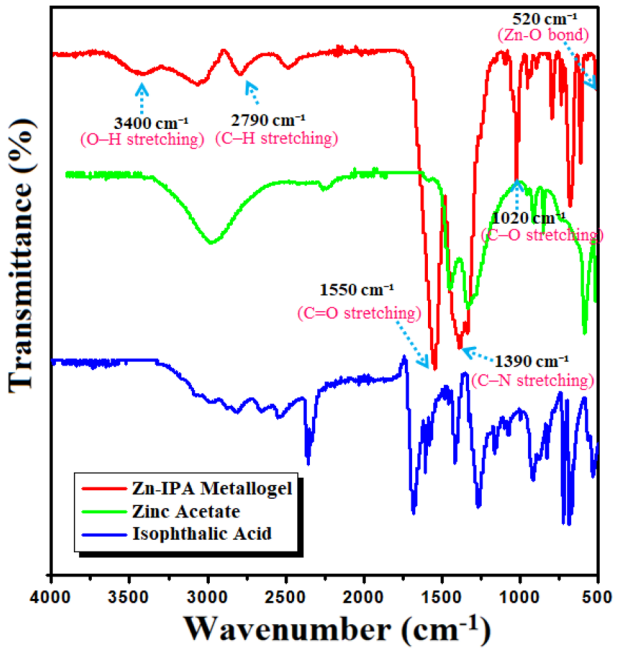

Fig. 4 FT-IR spectra of Zn-IPA metallogel in xerogel form, zinc acetate and isophthalic acid.

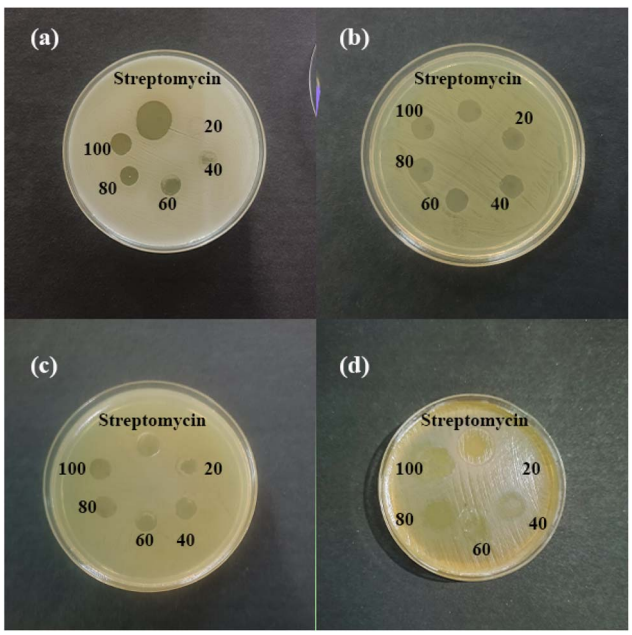

Fig. 5 Antimicrobial activity of Zn-IPA across a series of concentrations against four bacterial strains (a) *B. subtilis* (b) *S. epidermidis* (c) *E. coli* and (d) *P. aeruginosa*.

medium. Streptomycin (10 μL) and Zn-IPA at different concentration (10 μL) were spotted on agar surface to check antimicrobial activity against four bacterial strains. Simultaneously, antimicrobial activity of 2 mM IPA (10 μL) was also checked. The plates were incubated at 37 °C for 24 hours. The experiment was carried out in triplicates.

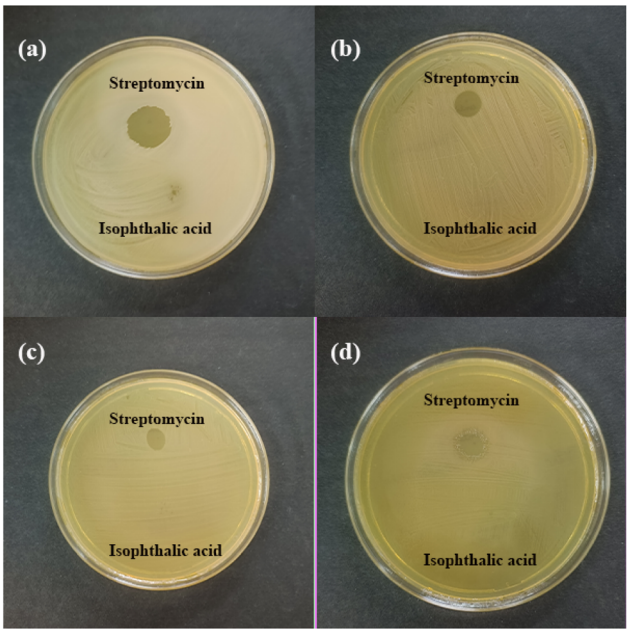

Fig. 6 No zone of inhibition of 2 mM isophthalic acid against four bacterial strains (a) *B. subtilis* (b) *S. epidermidis* (c) *E. coli* and (d) *P. aeruginosa*.

3. Results and discussion

3.1. Rheological analysis

To evaluate the mechanical stability and viscoelastic nature of the Zn-IPA metallogel, rheological measurements were carried out by varying both angular frequency and strain. A key characteristic of gel-like materials is when the storage modulus (G') exceeds the loss modulus (G''), indicating solid-like behavior. The Zn-IPA metallogel displayed such viscoelastic characteristics, with G' consistently higher than G'' across the tested frequency range, confirming its semi-solid gel nature. As shown in Fig. 2a, the average storage modulus (G') was greater than 10^3 Pa, significantly surpassing the loss modulus (G''), indicating strong mechanical integrity and stability of the network structure. Additionally, the strain-sweep test conducted at a constant angular frequency of 6.283 rad s^{-1} (1 Hz) is presented in Fig. 2b. This measurement further supports the robustness of the metallogel under increasing deformation, highlighting its ability to withstand mechanical stress without structural breakdown.

3.2. Study of morphology

The morphological features of the Zn-IPA metallogel were examined using field-emission scanning electron microscopy (FESEM). The FESEM images (Fig. 3a–d) revealed agglomerated mud-like formations. This characteristic microarchitecture arises from the supramolecular interactions between zinc acetate dihydrate [$Zn(CH_3COO)_2 \cdot 2H_2O$] and isophthalic acid in the DMF medium. These non-covalent interactions promote the self-assembly of a three-dimensional network, contributing to the gel's mechanical stability and structure. To further confirm

Table 1 Antimicrobial activity of Zn-IPA metallogel

	Zone of inhibition (mm in diameter)					
		Concentration of Zn-IPA (mg ml^{-1})				
Bacterial strain	Streptomycin (100 μg ml^{-1})	20 mg ml^{-1}	40 mg ml^{-1}	60 mg ml^{-1}	80 mg ml^{-1}	100 mg ml^{-1}
B. subtilis (a)	15 ± 0.20	No zone	No zone	11 ± 0.21	11.2 ± 0.25	12 ± 0.18
S. epidermidis (b)	11 ± 0.11	10 ± 0.22	10 ± 0.21	10 ± 0.15	10 ± 0.11	10 ± 0.23
E. coli (c)	12 ± 0.05	10 ± 0.23	11 ± 0.12	11 ± 0.20	12 ± 0.14	12 ± 0.10
P. aeruginosa (d)	16.5 ± 0.13	No zone	11 ± 0.16	11 ± 0.22	14 ± 0.17	16 ± 0.25

the elemental composition, energy-dispersive X-ray spectroscopy (EDX) mapping was performed. The EDX analysis (Fig. 3e–i) confirmed the uniform distribution of key elements-carbon (C), nitrogen (N), oxygen (O), and zinc (Zn)-within the metallogel matrix. These findings provide strong evidence for the successful coordination and network formation in the Zn-IPA metallogel system. Please see the SI file for energy-dispersive X-ray spectroscopy spectra as Fig. S1.

3.3. FT-IR analysis of Zn-IPA metallogel

Fourier-transform infrared (FT-IR) spectroscopy was conducted to elucidate the molecular interactions and functional groups involved in the formation of the Zn-IPA metallogel in its xerogel form (Fig. 4). The FT-IR spectrum displays characteristic vibrational bands that confirm successful gel formation through supramolecular interactions between zinc acetate and isophthalic acid. A broad and intense absorption band at 3400 cm^{-1} corresponds to O–H stretching vibrations, indicative of hydroxyl groups, while the symmetric C–H stretching is observed at 2790 cm^{-1}. The strong absorption at 1550 cm^{-1} is attributed to the carboxyl C=O stretching, and also reflects zinc carboxylate formation, confirming coordination between Zn^{2+} ions and the carboxylate groups of IPA. Further, C–N and C–O stretching vibrations appear at 1390 cm^{-1} and 1020 cm^{-1}, respectively. Peak shifts at 1550 cm^{-1} and 3080 cm^{-1} further signify the presence of zinc acetate, while additional bands at 684 cm^{-1}, 1270 cm^{-1}, 1612 cm^{-1}, 1670 cm^{-1}, and 2972 cm^{-1} are consistent with the vibrational modes of isophthalic acid, indicating its effective integration into the gel matrix. The peak at 680 cm^{-1} corresponds to COO^- bending, and a distinct band at 520 cm^{-1} is assigned to Zn–O stretching, confirming metal–ligand coordination. Overall, the observed shifts in intensity and wavenumber from those of the individual components highlight strong supramolecular interactions and complex formation, which are essential for the structural integrity and stability of the Zn-IPA metallogel.

3.4. Inhibiting activity for pathogens

Zn-IPA showed antimicrobial activity against Gram-positive *B. subtilis*, *S. epidermidis* and Gram-negative *E. coli*, *P. aeruginosa* (Fig. 5). The absence of an inhibition zone in plates spotted with 2 mM IPA indicated that the antimicrobial activity observed with Zn-IPA was not attributable to the antimicrobial properties of IPA (Fig. 6). During the incubation period of 24 hours, the metallogel slowly dispersed throughout the agar medium. A clear, circular zone appeared, where the metallogel was concentrated enough to prevent bacterial growth. The size of the zone reflects how well the metallogel inhibits the growth of the tested microorganisms. The antimicrobial effect of the metallogel Zn-IPA was assessed with a series of concentrations against different bacterial strains. The result demonstrated a quantitative inhibitory effect of Zn-IPA on the bacterial strains with a varying efficacy (Table 1). Gram-positive bacteria *B. subtilis* showed moderate susceptibility to Zn-IPA. No significant inhibitory zone was observed at the lower concentrations of Zn-IPA on *B. subtilis*. However larger zone for the higher concentrations were recorded. *S. epidermidis* showed a uniform susceptibility to the metallogel throughout the series of concentrations with no significant increase of zone diameter with the concentration of metallogel. Gram-negative bacteria *P. aeruginosa* showed significant inhibition zone in the higher concentrations before decreasing progressively and showing no zone in the lowest concentration. *E. coli* again showed a consistent susceptibility throughout all the concentrations with a slide increase in the zone diameter at higher concentrations suggesting a moderate activity of the metallogel. Synthesized derivatives demonstrating inhibition zones comparable with the reference antibiotic hold promise as antimicrobial agents. The presence of a smaller inhibition zone than streptomycin does not rule out antimicrobial effects; it simply implies a lower effectiveness at the given concentration. This can be advantageous in controlled drug treatments where moderate inhibition is preferred. Another thing to consider is that potent antibiotics can sometimes contribute to antibiotic resistance, but a more measured approach may help maintain their efficacy over time. The antimicrobial efficacy of Zn-IPA on four bacterial strains is presented in Table 1.

4. Conclusions

In conclusion, this work reports the successful development of a novel Zn(II)-based metallogel synthesized through a simple and efficient route involving the direct mixing of zinc acetate with isophthalic acid followed by ultrasonication at ambient conditions. The resulting metallogel displayed distinct surface morphologies, as observed through FESEM imaging. Rheological measurements confirmed its excellent mechanical robustness, while FT-IR analysis revealed key insights into the molecular interactions governing gel formation. Importantly,

antibacterial assays demonstrated the metallogel's strong inhibitory activity against pathogenic bacteria, underlining its potential utility in biomedical and pharmaceutical applications. These findings highlight the promise of such supramolecular material in addressing urgent healthcare issues, particularly bacterial infections. The developed Zn-metallogel not only serves as a platform for next-generation antibacterial agents but also opens avenues for applications across other domains such as drug delivery, wound healing, and tissue engineering. The simplicity and scalability of the synthesis method make it attractive for broader technological adoption. Moving forward, further modifications and interdisciplinary studies could optimize these materials for targeted applications in healthcare, environmental safety, and smart material systems. This study lays the groundwork for impactful innovations that bridge material science with societal well-being.

Conflicts of interest

The authors declare no competing financial interests.

Data availability

The authors declare that the data supporting the findings of this study are available within the paper and its SI files. Should any raw data files be needed in another format they are available from the corresponding author upon reasonable request.

Energy-dispersive X-ray spectroscopy spectra as Fig. S1. See DOI: **https://doi.org/10.1039/d5ra03663a**.

Acknowledgements

S. S. is thankful to DST India, New Delhi for Inspire Fellowship (No. DST/inspire Fellowship/2022/IF220441). S. B. thankfully acknowledges DST Inspire Faculty Research Grant (Faculty Registration No. IFA18-CH304; DST/INSPIRE/04/2018/000329).

Notes and references

1 D. Tripathy, A. S. Gadtya and S. Moharana, *Polym.-Plast. Technol. Mater.*, 2023, **62**, 306–326.
2 S. Datta and S. Bhattacharya, *Chem. Soc. Rev.*, 2015, **44**, 5596–5637.
3 A. Pape, M. Bastings, R. Kieltyka, H. Wyss, I. Voets, E. Meijer and P. Dankers, *Int. J. Mol. Sci.*, 2014, **15**, 1096–1111.
4 S. Dhibar, H. Dahiya, K. Karmakar, S. Kundu, S. Bhattacharjee, G. C. Nayak, P. Karmakar, G. D. Sharma and B. Saha, *J. Mol. Liq.*, 2023, **370**, 121020.
5 K. Karmakar, A. Dey, S. Dhibar, R. Sahu, S. Bhattacharjee, P. Karmakar, P. Chatterjee, A. Mondal and B. Saha, *RSC Adv.*, 2023, **13**, 2561–2569.
6 S. Ganta and D. K. Chand, *Dalton Trans.*, 2015, **44**, 15181–15188.
7 G. Yu, X. Yan, C. Han and F. Huang, *Chem. Soc. Rev.*, 2013, **42**, 6697.
8 S. Dhibar, A. Dey, S. Majumdar, A. Dey, P. P. Ray and B. Dey, *Ind. Eng. Chem. Res.*, 2020, **59**, 5466–5473.
9 M. Shirakawa, N. Fujita and S. Shinkai, *J. Am. Chem. Soc.*, 2003, **125**, 9902–9903.
10 T.-A. Asoh and A. Kikuchi, *Chem. Commun.*, 2012, **48**, 10019.
11 X. Yang, H. Zhang, J. Zhao, Y. Liu, Z. Zhang, Y. Liu and X. Yan, *Chem. Eng. J.*, 2022, **450**, 138135.
12 A. Rajak and A. Das, *ACS Polym. Au*, 2022, **2**, 223–231.
13 Y. Xu, Q. Wu, Y. Sun, H. Bai and G. Shi, *ACS Nano*, 2010, **4**, 7358–7362.
14 S. Dhibar, A. Dey, S. Majumdar, D. Ghosh, A. Mandal, P. P. Ray and B. Dey, *Dalton Trans.*, 2018, **47**, 17412–17420.
15 J. W. Steed, *Chem. Soc. Rev.*, 2010, **39**, 3686.
16 K. Hanabusa, K. Hiratsuka, M. Kimura and H. Shirai, *Chem. Mater.*, 1999, **11**, 649–655.
17 A. Prathap and K. M. Sureshan, *Langmuir*, 2019, **35**, 6005–6014.
18 (*a*) S. Dhibar, A. Dey, D. Ghosh, S. Majumdar, A. Dey, P. P. Ray and B. Dey, *ACS Omega*, 2020, **5**, 2680–2689; (*b*) S. Dhibar, A. Dey, R. Jana, A. Chatterjee, G. K. Das, P. P. Ray and B. Dey, *Dalton Trans.*, 2019, **48**, 17388–17394; (*c*) S. Dhibar, A. Roy, P. Das, T. Sarkar, M. Goswami, S. Some, K. Karmakar, P. Ruidas, S. Bhattacharjee, T. O Ajiboye, A. S. Ray, K. Sarkar, S. J. Ray and B. Saha, *Mater. Adv.*, 2025, **6**, 1899–1913; (*d*) A. Roy, S. Dhibar, K. Karmakar, S. Bhattacharjee, B. Saha and S. J. Ray, *Sci. Rep.*, 2024, **14**, 13109; (*e*) S. Dhibar, A. Roy, T. Sarkar, P. Das, K. Karmakar, S. Bhattacharjee, B. Mondal, P. Chatterjee, K. Sarkar, S. J. Ray and B. Saha, *Langmuir*, 2024, **40**, 179–192; (*f*) K. Karmakar, A. Roy, S. Dhibar, S. Majumder, S. Bhattacharjee, B. Mondal, S. M. Rahaman, R. Saha, S. J. Ray and B. Saha, *ACS Appl. Electron. Mater.*, 2023, **5**(6), 3340–3349.
19 M.-O. M. Piepenbrock, G. O. Lloyd, N. Clarke and J. W. Steed, *Chem. Rev.*, 2010, **110**, 1960–2004.
20 (*a*) S. Dhibar, A. Dey, A. Dalal, S. Bhattacharjee, R. Sahu, R. Sahoo, A. Mondal, S. M. Rahaman, S. Kundu and B. Saha, *J. Mol. Liq.*, 2023, **370**, 121021; (*b*) S. Dhibar, S. Babu, A. Mohan, G. K. Chandra, S. Bhattacharjee, K. Karmakar, P. Karmakar, S. M. Rahaman, P. Predeep and B. Saha, *J. Mol. Liq.*, 2023, **375**, 121348; (*c*) S. Dhibar, B. Pal, K. Karmakar, S. Kundu, S. Bhattacharjee, R. Sahoo, S. M. Rahaman, D. Dey, P. P. Ray and B. Saha, *ChemistrySelect*, 2023, **8**, e202204214; (*d*) S. Dhibar, B. Pal, K. Karmakar, S. Roy, S. A. Hafiz, A. Roy, S. Bhattacharjee, S. J. Ray, P. P. Ray and B. Saha, *Nanoscale Adv.*, 2023, **5**, 6714–6723; (*e*) S. Dhibar, A. Dey, B. Mondal, K. Karmakar, A. Roy, S. Bhattacharjee, A. Trivedi, A. Mohan, R. Saha, P. Chatterjee, A. Mondal, T. O Ajiboye and B. Saha, *J. Sol-Gel Sci. Technol.*, 2025, **113**, 896–909; (*f*) S. Dhibar, A. Mohan, K. Karmakar, B. Mondal, A. Roy, S. Babu, P. Garg, P. Ruidas, S. Bhattacharjee, S. Roy, A. Bera, S. J. Ray, P. Predeep and B. Saha, *RSC Adv.*, 2024, **14**, 12829–12840; (*g*) A. Roy, S. Dhibar, S. Kumar, S. Some, P. Garg, P. Ruidas, S. Bhattacharjee, A. Bera, B. Saha and S. J. Ray, *Sci. Rep.*, 2024, **14**, 31619; (*h*) A. Roy, S. Dhibar, S. Kumar, K. Karmakar, P. Garg, P. Ruidas, S. Bhattacharjee, A. Bera, B. Saha and S. J. Ray, *Sci. Rep.*, 2024, **14**, 26848.

21 S. Ganta and D. K. Chand, *Dalton Trans.*, 2015, **44**, 15181–15188.
22 C. Po, Z. Ke, A. Y. Tam, H. Chow and V. W. Yam, *Chem.–Eur. J.*, 2013, **19**, 15735–15744.
23 B. Jiang, L.-J. Chen, G.-Q. Yin, Y.-X. Wang, W. Zheng, L. Xu and H.-B. Yang, *Chem. Commun.*, 2017, **53**, 172–175.
24 S. Das, M. Banik, G. Chen, S. Sinha and R. Mukherjee, *Soft Matter*, 2015, **11**, 8550–8583.
25 M. reza Saboktakin and R. M. Tabatabaei, *Int. J. Biol. Macromol.*, 2015, **75**, 426–436.
26 Y. Zhao, S. Song, X. Ren, J. Zhang, Q. Lin and Y. Zhao, *Chem. Rev.*, 2022, **122**, 5604–5640.
27 S. Sarkar, S. Dutta, S. Chakrabarti, P. Bairi and T. Pal, *ACS Appl. Mater. Interfaces*, 2014, **6**, 6308–6316.
28 A. R. Hirst, B. Escuder, J. F. Miravet and D. K. Smith, *Angew. Chem., Int. Ed.*, 2008, **47**, 8002–8018.
29 S. Dhibar, A. Dey, A. Dey, S. Majumdar, D. Ghosh, P. P. Ray and B. Dey, *ACS Appl. Electron. Mater.*, 2019, **1**, 1899–1908.
30 S. Dhibar, S. K. Ojha, A. Mohan, S. P. C. Prabhakaran, S. Bhattacharjee, K. Karmakar, P. Karmakar, P. Predeep, A. K. Ojha and B. Saha, *New J. Chem.*, 2022, **46**, 17189–17200.
31 (*a*) B. Pal, S. Dhibar, R. Mukherjee, S. Bhattacharjee, P. P. Ray and B. Saha, *Mater. Adv.*, 2023, **4**, 3628–3635; (*b*) S. Dhibar, S. K. Ojha, K. Karmakar, P. Karmakar, S. Bhattacharjee, P. Chatterjee, A. K. Ojha and B. Saha, *Chem. Afr.*, 2023, **6**, 3217–3228.
32 S. Dhibar, S. Babu, K. Karmakar, A. Mohan, S. Bhattacharjee, S. M. Rahaman, G. C. Nayak, R. Saha, P. Predeep and B. Saha, *Chem. Phys. Lett.*, 2023, **829**, 140777.
33 A. Roy, S. Dhibar, K. Karmakar, S. Some, S. A. Hafiz, S. Bhattacharjee, B. Saha and S. J. Ray, *Mater. Adv.*, 2024, **5**, 3459–3471.
34 J. Chen, T. Wang and M. Liu, *Inorg. Chem. Front.*, 2016, **3**, 1559–1565.
35 S. Dhibar, S. Pal, K. Karmakar, S. A. Hafiz, S. Bhattacharjee, A. Roy, S. K. M. Rahaman, S. J. Ray, S. Dam and B. Saha, *RSC Adv.*, 2023, **13**, 32842–32849.
36 (*a*) S. Dhibar, S. Pal, S. Some, K. Karmakar, R. Saha, S. Bhattacharjee, A. Roy, S. J. Ray, T. O. Ajiboye, S. Dam and B. Saha, *RSC Adv.*, 2024, **14**, 26354–26361; (*b*) S. Dhibar, A. Mohan, S. Some, K. Karmakar, S. Babu, S. Bhattacharjee, S. J. Ray, L. N. Nthunya, T. O Ajiboye, P. Predeep and B. Saha, *Discov Mol.*, 2025, **2**, 11; (*c*) S. Dhibar, S. Pal, S. Some, K. Karmakar, R. Saha, S. Bhattacharjee, D. Kumari, A. Mohan, T. O. Ajiboye, S. J. Ray, S. Roy, S. Dam and B. Saha, *RSC Adv.*, 2025, **15**, 5214–5219.
37 W.-L. Guan, K. M. Adam, M. Qiu, Y.-M. Zhang, H. Yao, T.-B. Wei and Q. Lin, *Supramol. Chem.*, 2020, **32**, 578–596.
38 E. M. M. Ibrahim, L. H. Abdel-Rahman, A. M. Abu-Dief, A. Elshafaie, S. K. Hamdan and A. M. Ahmed, *Mater. Res. Bull.*, 2018, **107**, 492–497.
39 E. M. M. Ibrahim, L. H. Abdel-Rahman, A. M. Abu-Dief, A. Elshafaie, S. K. Hamdan and A. M. Ahmed, *Mater. Res. Bull.*, 2018, **107**, 492–497.
40 P. Sutar and T. K. Maji, *Inorg. Chem.*, 2017, **56**, 9417–9425.
41 P. Biswas and P. Dastidar, *Inorg. Chem.*, 2021, **60**, 3218–3231.
42 M. Tao, K. Xu, S. He, H. Li, L. Zhang, X. Luo and W. Zhong, *Chem. Commun.*, 2018, **54**, 4673–4676.
43 A. Biswas, S. Mukhopadhyay, R. S. Singh, A. Kumar, N. K. Rana, B. Koch and D. S. Pandey, *ACS Omega*, 2018, **3**, 5417–5425.
44 M. Wang, S. Day, Z. Wu, X. Wan, X. Ye and B. Cheng, *Colloids Surf., A*, 2021, **628**, 127335–127347.
45 Y. Shi, M. Wang, C. Ma, Y. Wang, X. Li and G. Yu, *J. Nanosci. Lett.*, 2015, **15**, 6276.
46 L. Qin, P. Wang, Y. Guo, C. Chen and M. Liu, *Adv. Sci.*, 2015, **2**, 1500134.
47 P. Bairagi, P. Ghosh, P. Roy and A. Banerjee, *ACS Appl. Nano Mater.*, 2023, **6**, 2299–2309.
48 H. T. P. Anh, C.-M. Huang and C.-J. Huang, *Sci. Rep.*, 2019, **9**, 11562.
49 G. Lepcha, B. Pal, S. Majumdar, K. T. Ahmed, I. Pal, S. R. Biswas, P. P. Ray and B. Dey, *Mater. Adv.*, 2023, **4**, 2595–2603.
50 G. Lepcha, S. Majumdar, B. Pal, K. T. Ahmed, I. Pal, B. Satpati, S. R. Biswas, P. P. Ray and B. Dey, *Langmuir*, 2023, **39**, 7469–7483.
51 M. Khan, A. H. Naqvi and M. Ahmad, *Toxicol Rep*, 2025, **2**, 765–774.
52 J. Borovanský and P. A. Riley, *Chem.-Biol. Interact.*, 1989, **69**, 279–291.